POAC'13
Espoo, Finland

Proceedings of the 22nd International Conference on
Port and Ocean Engineering under Arctic Conditions
June 9-13, 2013
Espoo, Finland

Effects of Pre-Strain on the Elastic Properties and the Ductile-to-Brittle Transition of Columnar Ice

Scott A. Snyder, Erland M. Schulson, Carl E. Renshaw

Ice Research Laboratory, Thayer School of Engineering, Dartmouth College
Hanover, NH 03755 U.S.A.

ABSTRACT

Experiments on ice at $-10\,^{\circ}\mathrm{C}$ reveal changes to its elastic properties and ductile-to-brittle transition due to prior damage imparted during plastic strain. Polycrystalline columnar S2 ice was grown in the laboratory to simulate both naturally-grown fresh-water ice and sea ice. Cubic specimens of the ice were initially compressed uniaxially across the columnar grains up to 10% strain at a rate of $10^{-5}\,\mathrm{s}^{-1}$ or $10^{-4}\,\mathrm{s}^{-1}$, generating damage in two forms: 1) non-propagating wing cracks and transgranular cracks, and 2) recrystallized grains. Elastic properties in two across-column directions, both parallel (x_1) and perpendicular (x_2) to the initial loading direction, were obtained from *P*–wave and *S*–wave ultrasonic velocities. The specimens were then individually reloaded uniaxially at a strain rate ranging from $10^{-5}\,\mathrm{s}^{-1}$ to $10^{-1}\,\mathrm{s}^{-1}$.

As a result of the pre-strain damage in both materials, elastic moduli were reduced by up to 30%; the ductile-to-brittle transition strain rate was increased up to a factor of 3 to 10; and the ductile behavior with respect to loading along a direction within the horizontal (x_1-x_2) plane of the parent ice sheet changed from isotropic to anisotropic. For fresh-water ice pre-strained by 10%, the ductile-to-brittle transition was observed to occur at a strain rate ($10^{-3}\,\mathrm{s}^{-1}$) of about one order of magnitude higher than for undamaged ice. The transition strain rate was observed to increase by a lesser amount in saline ice similarly pre-strained at $10^{-5}\,\mathrm{s}^{-1}$, but by a comparable amount in saline ice pre-strained at $10^{-4}\,\mathrm{s}^{-1}$. As the rate at which pre-strain is imparted approaches the ductile-to-brittle transition strain rate of the undamaged material, the magnitude of pre-strain effects appears to increase. The nature of these effects is discussed.

1 INTRODUCTION

The design of offshore structures in arctic conditions relies on an understanding of the mechanical properties and behavior of ice. Under compression, the macroscopic behavior changes from ductile to brittle at a critical strain rate that depends on a number of factors (for review see Schulson and Duval, 2009). This transition is important for at least two reasons. First, the strength of ice—and thus the load it exerts on a vertical-sided structure—can reach a maximum at the ductile-to-brittle transition strain rate. Second, above this transition rate, ice fails by brittle fracture with an abrupt drop in load-bearing ability, causing whatever structure against which it has been compressed to spring back. Yet the ice may continue to advance into the structure, reloading again with potentially dangerous vibrations developing as the process repeats (Sodhi, 2001). A broader implication of repetitive loading is that ice arrives with a mechanical history. Previous work has investigated the ductile-to-brittle transition, for example, as a function of temperature (Qi and Schulson, 1998) or of confinement (Schulson and Buck, 1995), but in each case treating ice as a virgin material. Does the ductile-to-brittle transition depend on the prior

straining of ice, which may leave permanent change in its microstructure or damage in the form of cracks? Does prior strain damage affect other material properties, such as elastic moduli? This paper reports results from new experiments that have been conducted on both fresh-water and salt-water ice, grown and tested at $-10\,^{\circ}\mathrm{C}$ in the laboratory, with the aim to ascertain the effects of uniaxially compressive pre-strain on the elastic moduli and on the ductile-to-brittle transition.

2 EXPERIMENTAL PROCEDURE

The project involves growing and preparing ice specimens, loading the specimens to impart pre-strain damage, obtaining elastic properties using ultrasonic transmission techniques, and finally reloading the specimens to failure. The procedures for these steps are summarized below:

2.1 Ice preparation

Polycrystalline columnar ice was grown in the laboratory to simulate both naturally-grown fresh-water ice and sea ice. Fresh-water ice was grown over filtered tap water. Salt-water ice was grown over a 17.5 ppt saline solution prepared from "Instant Ocean", a commercial mixture whose composition reflects that of sea salts. The ice was grown in one of two cylindrical polyethylene tanks, either a large (800 L) tank or a smaller (57 L) tank, which were wrapped with insulation on the sides to promote unidirectional freezing. After filling the tank, the water or solution was allowed to equilibrate to $4\,^{\circ}\mathrm{C}$ and damp mixing currents for saline ice. The liquid surface was seeded with a layer of $< 4\,\mathrm{mm}$ equiaxed fresh-water ice grains. Immediately after seeding, the tank was capped with a cooling plate of aluminum set in contact with the liquid surface and built with internal channels to circulate a glycol-water coolant pumped from a refrigerated bath. The plate was maintained at $-20\,^{\circ}\mathrm{C}$ until ice of both kinds had formed to a depth of 22 cm to 30 cm.

Thin-section examination of both the saline and fresh-water ice using a Rigsby stage confirmed the S2 growth texture (where the crystallographic c-axes are essentially confined to the horizontal plane, i.e. normal to the direction of freezing, but are randomly oriented within this plane), which commonly occurs in natural ice covers.

To prepare for testing, the ice was machined into 6-inch ($(152.0 \pm 0.1)\,\mathrm{mm}$) cubes using a horizontal mill, taking care to align one edge of the cube parallel to the long axis of the columnar grains, identified as the x_3 direction. The density of each specimen was taken by weighing the mass of the cube and dividing by volume as the product of measured lengths in each direction.

2.2 Pre-straining procedure

The cubic specimens at a temperature of $(-10.0 \pm 0.2)\,^{\circ}\mathrm{C}$ were loaded in uniaxial compression in the x_1 across-column direction to impart a specified level of pre-strain, ε_p, at a constant strain rate, $\dot{\varepsilon}_\mathrm{p}$ (typically $10^{-5}\,\mathrm{s}^{-1}$, plus additional tests on saline ice at $10^{-4}\,\mathrm{s}^{-1}$). Pre-strains of -0.003, -0.035, and -0.10 were specified as levels that could produce plastic deformation but keep the specimen intact. Loading was performed on a servo-hydraulic multi-axial test system (MATS) using the pair of vertical actuators. In order to minimize lateral confinement on its loaded (x_1) faces, the specimen was placed between brass brush platens fastened to the load cell attached to each actuator. The other faces of the specimen were unconfined. After being pre-strained, the specimen was re-milled to square its faces; particularly the x_2 face had noticeable deformation after loading.

2.3 Assessment of pre-strain damage

The pre-straining process generated damage in the form of recrystallized grains as well as non-propagating cracks that were detected both acoustically during loading and visually after unloading. Acoustic emissions (AE) were monitored during pre-straining using a piezoelectric transducer frozen directly to the side of the specimen. Recorded AE activity correlated strongly with visible cracking in both kinds of ice. For fresh-water ice pre-strained at $10^{-5}\,\mathrm{s}^{-1}$, cracking

activity began slowly, then accelerated to a peak rate around 0.5 % strain, began to level off around 3.5 % strain, and finally became scarcely detectable by the time the specimen had shortened by 10 %. Crack activity in saline ice pre-strained at $10^{-5}\,\mathrm{s}^{-1}$ followed a similar pattern, but with fewer cracks generated.

Thin sections from the pre-strained specimens were prepared to visually assess the damage (Figure 1). Counting the number of cracks proved especially difficult in saline ice due to the presence of brine platelets and air bubbles in the thin sections. Crack development was more visible in thin sections of fresh-water ice, in which two types of cracks were observed: 1) transgranular cracks, the lengths of which were essentially limited by the columnar grain diameter 3 mm to 12 mm, and 2) cracks where decohesion had occurred at grain boundaries. Due to the columnar grains, the intergranular cracks typically had highly-attenuated, non-square proportions. Standard methods for quantifying a damage parameter assume small (relative to specimen length) cracks of roughly square proportions for simplicity (Lemaitre, 1996). Crack density was estimated by inspecting thin-sections of the damaged specimen. For 3.5 % pre-strain, crack density averaged between 0.03 to 0.05 volume fraction. Thin sections were also photographed with cross-polarized light, revealing greater degrees of recrystallization with increasing levels of pre-strain.

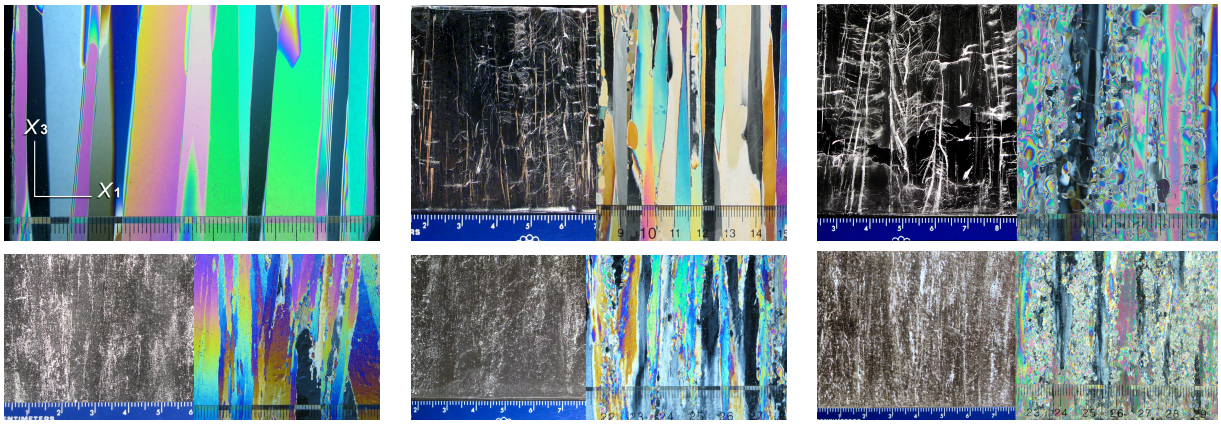

undamaged pre-strained 3.5% pre-strained 10%

Figure 1: Thin sections of fresh-water ice (top row) and saline ice (bottom row) at −10 °C for $\dot{\varepsilon}_\mathrm{p} = 10^{-5}\,\mathrm{s}^{-1}$ for various levels of pre-strain. Smallest feature size on scale is 1 mm.

2.4 Measurement of elastic properties

The density of the re-milled specimen was measured again in the same way, capturing within the measurement of its bounding volume any porous space of cracks imparted through pre-straining. Next, the specimen was sectioned into rectangular prisms (6 cm square × 12 cm) with the long dimension running across the columnar grains either parallel (x_1) or perpendicular (x_2) to the initial loading direction. Elastic properties in both the x_1 and x_2 directions were then determined from specimen density, ρ, and from *P*–wave (longitudinal) and *S*–wave (transverse, or shear) ultrasonic velocities. The dimensions and density of each subspecimen were measured likewise.

Ultrasonic measurements were performed using a through-transmission setup that had been calibrated using aluminum samples of both prismatic and cylindrical shapes, as well as using undamaged ice of both kinds. *P*–wave and *S*–wave speeds, c_P and c_S respectively, were found by manually determining the first-arrival times of a pulse transmitted through the specimen between a pair of ultrasonic transducers, and dividing into the specimen length. The elastic Young's modulus, E, shear modulus, G, Poisson's ratio, ν, and bulk modulus, B, can be calculated using the following relations:

$$E = \rho c_S^2 \frac{(3c_P^2 - 4c_S^2)}{(c_P^2 - c_S^2)} \qquad (1)$$

$$G = \rho c_S^2 \qquad (2)$$

$$\nu = \frac{(c_P^2 - 2c_S^2)}{2(c_P^2 - c_S^2)} \qquad (3)$$

$$B = (\rho/3)(3c_P^2 - 4c_S^2) \qquad (4)$$

Two aspects of this ultrasonic measurement method deserve mention. First, the above equations assume an isotropic material, which columnar ice is not. The polycrystalline parent specimens and subspecimens were made as large as the loading apparatus and ultrasonic transducers could accommodate in order to minimize orientation effects of any single grain within the bulk sample. Static methods that obtain elastic modulus from the displacement under an applied stress were not used in these tests, in order to avoid inaccuracies due to creep and observed dependence on strain rate in compression tests (Vaudrey, 1977). Our use of the ultrasonic technique was validated by the close match between results from our calibration tests on as-grown specimens and previously published properties of fresh-water ice (Gammon et al., 1983) and sea ice (Sinha, 1989). Second, the accuracy of choosing the pulse first-arrival times is subject to signal noise, which may increase with damage, and to user error. The uncertainty in the measured wave speeds is estimated to be $\pm 5\,\%$, while the standard deviation in calculated properties was seldom less than $2\,\%$. Given these limitations, the measurement of elastic properties reported herein was intended to broadly discern the magnitude of pre-strain effects, if any.

2.5 Reloading procedure

Finally, the rectangular prisms milled from the pre-strained parent specimen were individually reloaded at $-10\,^{\circ}\mathrm{C}$ at a constant strain rate, $\dot{\varepsilon}_{\mathrm{r}}$, ranging from 10^{-5} to $10^{-2}\,\mathrm{s}^{-1}$, compressing uniaxially in the long dimension. In order to minimize boundary confinement, a thin ($\sim 0.15\,\mathrm{mm}$) sheet of polyethylene was placed between the subspecimen and each loading platen. The elapsed time between pre-straining and reloading was held constant at $(24 \pm 4)\,\mathrm{h}$.

Following the procedures just described, the first set of experiments was performed on fresh-water ice, pre-straining by $3.5\,\%$ and reloading up to an additional $3.5\,\%$. These were followed by similar tests on saline-ice, for a range of pre-strain levels, extending the reloading up to $10\,\%$ shortening in order to better observe the range of ductile behavior, as will be explained further. The procedures used for measuring elastic properties and reloading were also performed for comparison on similarly-sized prismatic specimens milled from undamaged ice of both types.

3 RESULTS AND DISCUSSION

3.1 Density and elastic properties

In both types of ice at $-10\,^{\circ}\mathrm{C}$, the arrival times of both *P*– and *S*–wave pulses increased detectably with increasing levels and rates of pre-strain, implying a reduction in wave velocity and, correspondingly, a reduction in stiffness of the ice. Likewise, the mass density decreased with increasing pre-strain. We observe that pre-strain reduced the density and elastic moduli by a greater amount in fresh-water ice than in saline ice under the same pre-strain conditions. Furthermore, for both types of ice, similar pre-strain imparted along the x_1 direction tended to cause a greater reduction in elastic moduli measured along x_2, ranging from slightly more than up to twice as much as those measured along x_1. Pre-strain generally showed little to no detectable effect on Poisson's ratio. Table 1 lists the properties and the direction in which they were measured for both as-grown and pre-strained ice. Density and elastic moduli depend also on the rate at which pre-strain is applied, as seen in saline ice, for example, the properties of which were more reduced by pre-straining at a higher rate of $1 \times 10^{-4}\,\mathrm{s}^{-1}$. The effects of pre-strain level on density, Young's modulus, and shear modulus are illustrated in Figure 2.

Table 1: Summary of density and elastic properties at $-10\,^{\circ}\mathrm{C}$ of fresh-water ice (upper rows) and saline ice (lower rows) for various levels of pre-strain.

MATERIAL			Measured Properties (± sample standard deviation)					
			n	ρ	ν	E	B	G
Pre-strain rate	Specimen orientation	Level of pre-strain in X_1	samples	Density / kg·m^{-3}	Poisson's Ratio	Young's Modulus / GPa	Bulk Modulus / GPa	Shear Modulus / GPa
FRESH-WATER ICE		0	5	915.9 ± 1.2	0.33 ± 0.01	9.60 ± 0.25	9.31 ± 0.34	3.62 ± 0.12
10^{-5} s^{-1}	X_1	0.035	10	886.9 ± 12.2	0.33 ± 0.01	8.33 ± 0.34	8.08 ± 0.42	3.14 ± 0. 14
		0.100	8	860.8 ± 3.2	0.34 ± 0.01	7.22 ± 0.10	7.28 ± 0.31	2.71 ± 0.04
	X_2	0.035	12	894.5 ± 11.0	0.32 ± 0.01	7.38 ± 0.30	6.63 ± 0.30	2.81 ± 0. 12
		0.100	7	865.0 ± 3.6	0.32 ± 0.03	5.76 ± 0.15	5.48 ± 0.95	2.18 ± 0.04
SALINE ICE		0	18	902.5 ± 13.4	0.34 ± 0.00	8.25 ± 0.42	8.58 ± 0.38	3.08 ± 0.16
10^{-5} s^{-1}	X_1	0.003	4	905.3 ± 3.6	0.34 ± 0.01	8.25 ± 0.15	8.62 ± 0.25	3.08 ± 0.06
		0.035	16	901.5 ± 3.8	0.34 ± 0.01	7.92 ± 0.40	8.06 ± 0.36	2.96 ± 0.1 6
		0.100	8	879.2 ± 5.4	0.34 ± 0.00	7.27 ± 0.13	7.47 ± 0.12	2.72 ± 0.06
	X_2	0.003	5	903.9 ± 5.8	0.34 ± 0.00	8.11 ± 0.14	8.38 ± 0.23	3.03 ± 0.05
		0.035	14	905.6 ± 2.5	0.34 ± 0.00	7.43 ± 0.35	7.58 ± 0.42	2.78 ± 0.1 3
		0.100	10	886.1 ± 2.3	0.33 ± 0.01	7.29 ± 0.16	7.32 ± 0.40	2.73 ± 0.0 7
10^{-4} s^{-1}	X_1	0.100	4	861.5 ± 9.8	0.33 ± 0.01	6.90 ± 0.15	7.09 ± 0.42	2.59 ± 0.06
	X_2	0.100	4	869.0 ± 1.2	0.33 ± 0.01	6.53 ± 0.04	6.43 ± 0.18	2.45 ± 0.02

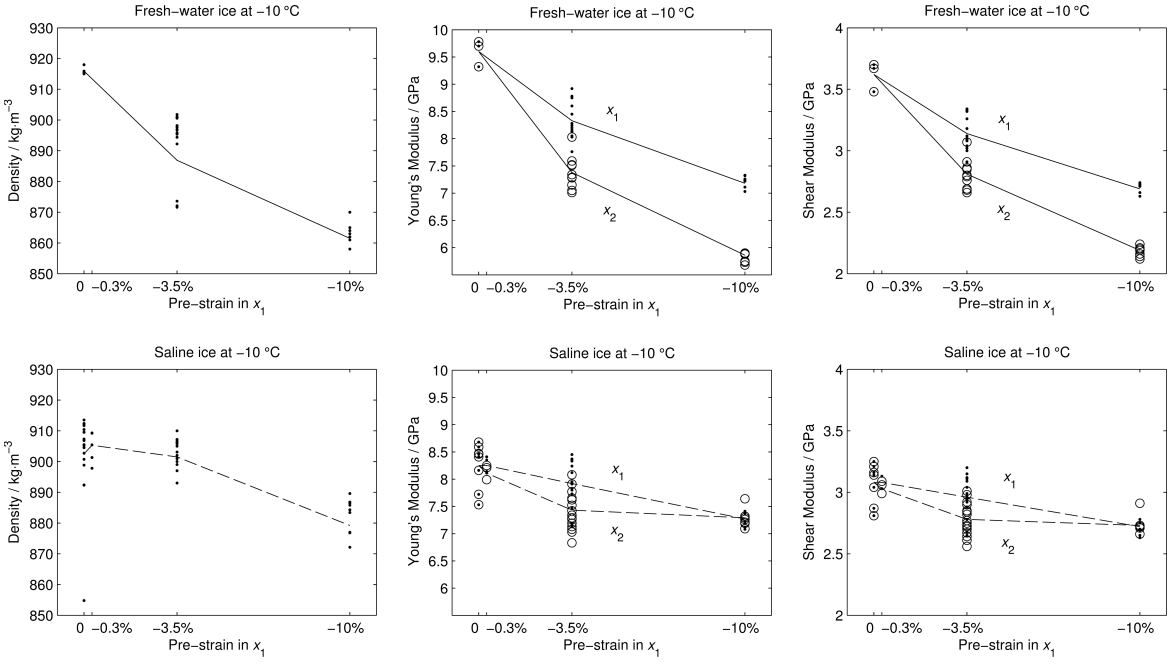

Figure 2: Density and elastic moduli of fresh-water ice (upper graphs) and saline ice (lower graphs) at $-10\,^{\circ}\mathrm{C}$ as functions of applied pre-strain at $1 \times 10^{-5}\,\mathrm{s}^{-1}$. Lines connect mean values of measurements.

3.2 Ductile-to-brittle transition

When the specimens were reloaded, they exhibited a range of ductile to brittle behavior depending upon strain rate. At high rates of strain, brittle failure occurred either by axial cleavage (splitting along one or more planes parallel to the direction of loading) or by fracturing along a shear fault. At lower strain rates, macroscopically ductile behavior was observed, characterized by the persistence of plastic deformation. However, in attempts to distinguish ductile from brittle

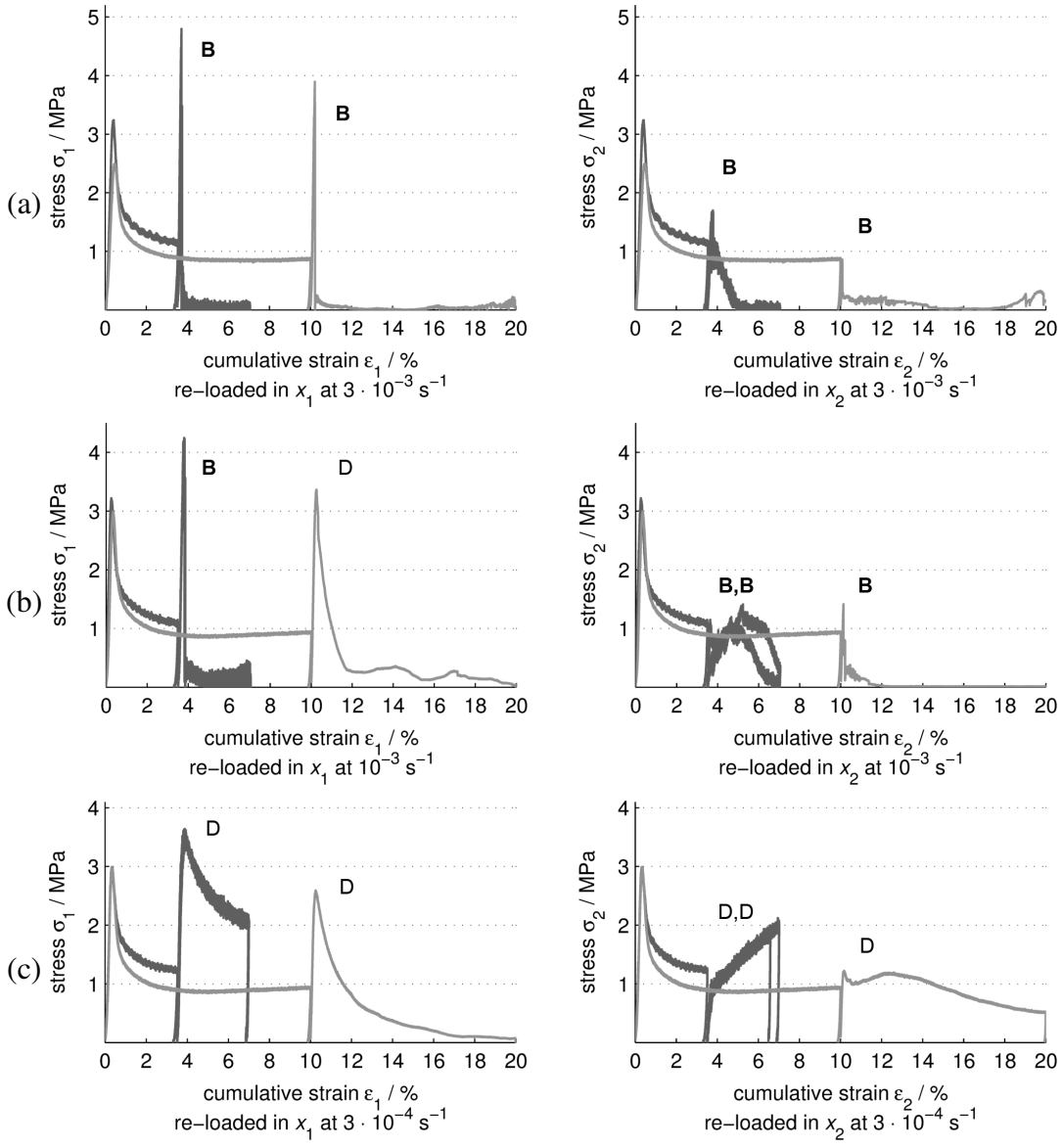

Figure 3: Fresh-water ice: graphs of nominal stress versus cumulative strain, combining curves for pre-straining (in x_1 at $10^{-5}\,\mathrm{s}^{-1}$) and reloading (in direction and at rate as shown for each subplot) at $-10\,^{\circ}\mathrm{C}$. Elapsed time between pre-straining and reloading was $(24 \pm 4)\,\mathrm{h}$.

behavior, the macroscopic appearance of the deformed ice could be misleading. At strain rates just below that which caused sudden brittle failure, in some cases, as plastic deformation proceeded, certain cracks might fortuitously align and connect to cause portions of the specimen to fracture away. In other cases, the specimen remained intact, albeit severely cracked, throughout reloading up to the terminal $10\,\%$ strain.

A more consistent characterization of ductile versus brittle behavior can be made by examining the stress-strain curves, shown in Figures 3 and 4 for pre-strained fresh-water and saline ice, respectively. These figures plot the axial stress, σ, recorded during reloading adjacent to that recorded during pre-straining (keeping in mind that, in most cases, the pre-shortening would have been applied at a different strain rate), in order to show the full stress history of the specimen in terms of cumulative strain. The plots are paired with reloading in x_1 on the left and reloading in x_2 on the right. Tests run under the same conditions are overlayed to demonstrate the reproducibility of the behavior.

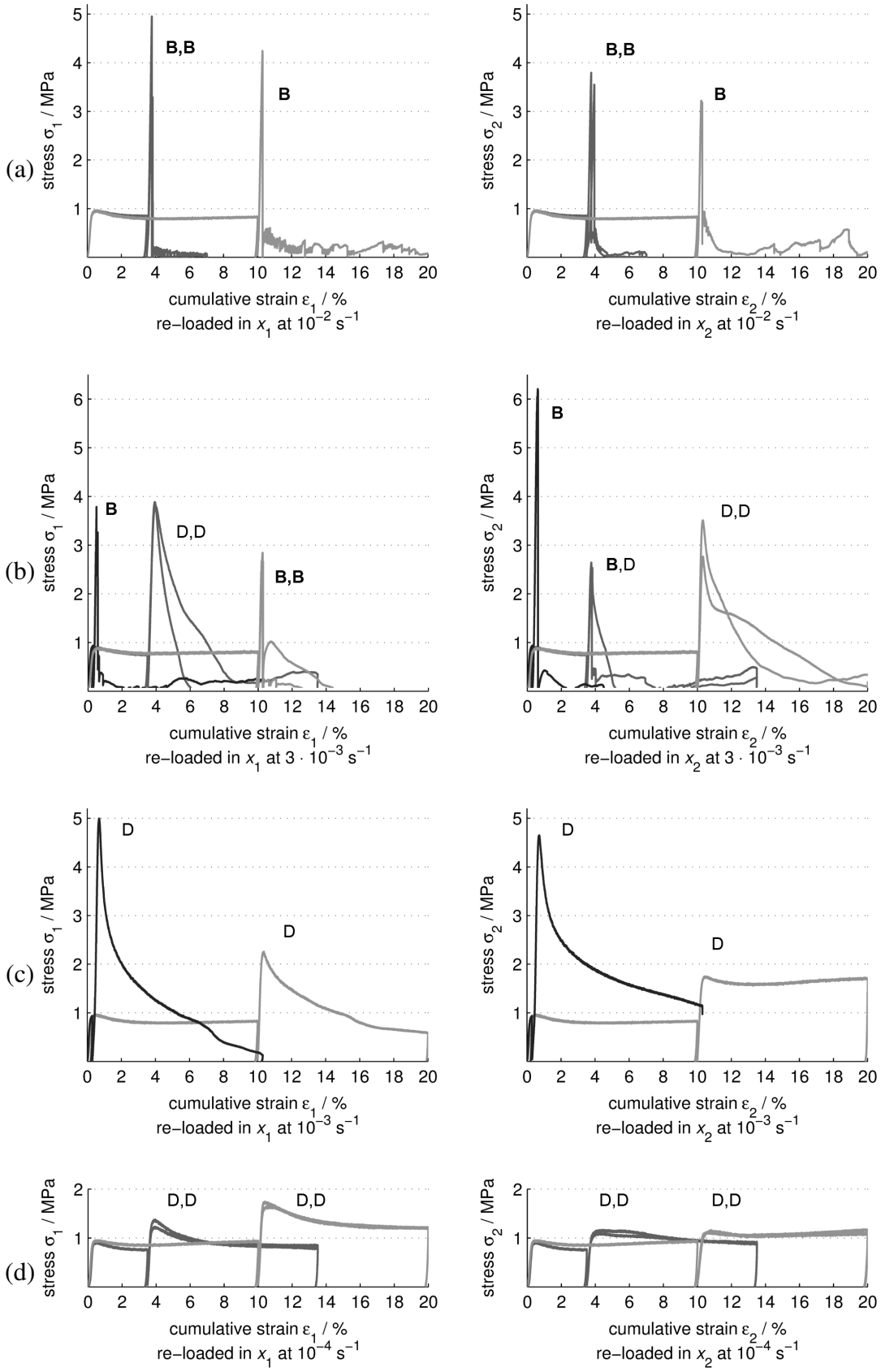

Figure 4: Saline ice: graphs of nominal stress versus cumulative strain, combining curves for pre-straining (in x_1 at $10^{-5}\,\mathrm{s}^{-1}$) and reloading (in direction and at rate as shown for each subplot) at $-10\,^{\circ}\mathrm{C}$. Elapsed time between pre-straining and reloading was $(24 \pm 4)\,\mathrm{h}$.

Both modes of brittle failure (axial cleavage and shear faulting) were marked by a sharp peak, σ_{max}, in the stress-strain curve followed by an abrupt drop in axial stress, $-\Delta\sigma$, as seen at high $\dot{\varepsilon}_r$, for example in all reloading curves of Figure 4(a). As $\dot{\varepsilon}_r$ decreases, the reloading curves tended to become less peaked as stress dropped less abruptly. At the lowest reloading strain rates, e.g., Figure 4(d), an essentially steady-state strain condition developed near the same level of stress reached at the end of pre-straining. Based on these observations, we have defined the macroscopic mechanical behavior quantitatively as:

Brittle– when $-\Delta\sigma > 0.5\,\sigma_{max}$ within 0.1% strain after the peak stress, σ_{max}, occurs,

and

Ductile– otherwise, i.e., when σ remains $> 0.5\,\sigma_{max}$ beyond 0.1% strain after peak.

Within the ductile regime, therefore, weakening to various degrees may occur over several percent additional strain, whereas brittle behavior is distinguished by sudden and catastrophic loss of strength. These definitions are made from a macroscopic point of view, cognizant of observations that correlate bulk material behavior to the localization of damage (Weiss, 2001). Table 2 summarizes the observations on the character of mechanical behavior—ductile versus brittle as defined above—for the pre-strain and reloading conditions tested. These results were reproducible and fairly insensitive to the defined $\Delta\sigma/\sigma_{max}$ ratio. Note the inherent difference between the undamaged (0 pre-strain) transition strain rates for fresh-water ice ($\sim 1\times10^{-4}\,s^{-1}$) and saline ice ($\sim 1\times10^{-3}\,s^{-1}$).

Table 2: Mechanical behavior—denoted as ductile (D) or brittle (**B**)—of ice at $-10\,^{\circ}C$ at various levels of pre-strain and rates of reloading in x_1. Ductile specimens remained intact upon reloading to additional compressive strain of 0.100, unless noted otherwise.

Material and pre-strain rate	Pre-strain in X1	Re-loading strain rate / s^{-1}								
		10^{-5}	$3x10^{-5}$	10^{-4}	$3x10^{-4}$	10^{-3}	$3x10^{-3}$	10^{-2}	$3x10^{-2}$	10^{-1}
Fresh-water ice	0**	D	D	D	**B**	**B**	**B**			
$10^{-5}\,s^{-1}$	0.035			D	D	**B**	**B**	**B**		
	0.100				D	D	**B**	**B**		
Saline ice	0	D		D	D*	D, **B**	**B***	**B**	**B**	**B**
	0.003					D	**B**			
	0.005*	D				D	**B**			
$10^{-5}\,s^{-1}$	0.010*	D				D	**B**			
	0.035	D		D		D*	D	**B**	**B***	
	0.100	D		D		D	**B**	**B**		
$10^{-4}\,s^{-1}$	0.100						D	**B**		

'D,**B**' indicates that both behaviors were observed in separate specimens loaded under the same conditions.
* Previous data from (Kuehn et al., 1988). ** Previous data from (Schulson and Buck, 1995).

The data from Table 2 are plotted in Figure 5. On each graph, the broken line marks the boundary between ductile behavior below and brittle behavior above, identifying the transition strain rate, $\dot{\varepsilon}_{DB}$, and highlighting its sensitivity to ε_p. In pre-strained fresh-water ice (Figure 5a), the transition from ductile to brittle failure was observed to occur at higher rates ($\dot{\varepsilon}_{DB} > 3\times10^{-4}\,s^{-1}$ for $\varepsilon_p = 3.5\,\%$, and $\dot{\varepsilon}_{DB} > 1\times10^{-3}\,s^{-1}$ for $\varepsilon_p = 10\,\%$) than for undamaged fresh-water ice. In saline ice pre-strained at $1\times10^{-5}\,s^{-1}$ (Figure 5b), the shift in $\dot{\varepsilon}_{DB}$ due to pre-strain appeared less than the shift observed in fresh-water ice.

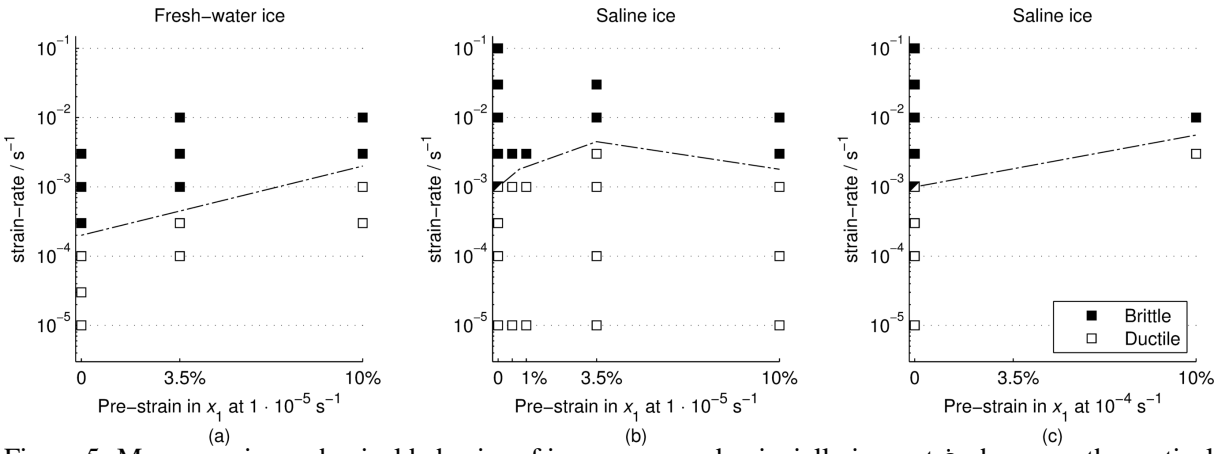

Figure 5: Macroscopic mechanical behavior of ice compressed uniaxially in x_1 at $\dot{\varepsilon}_r$ shown on the vertical axis, after being pre-strained to ε_p, shown on the horizontal axis. (Half-shaded squares indicate both ductile and brittle modes were observed in multiple specimens loaded under the same conditions.)

Based on comparing Figures 5 (a) and (b), the ductile-to-brittle transition may appear more sensitive to pre-strain in fresh-water ice than in saline ice. We caution the reader from attributing this to a fundamental difference in materials. In fact, although the pre-strain rates applied in these experiments were nominally identical at $10^{-5}\,\mathrm{s}^{-1}$, it is important to notice that this rate is closer in magnitude to the inherent ductile-to-brittle transition of undamaged fresh-water ice than to that of undamaged salt-water ice.

The effects of pre-strain appear to depend on the relative rate at which it is applied. At root are two competing mechanisms: the propagation of cracks and the generation of dislocations from crack tips (Schulson and Duval, 2009). The former underlies brittleness; the latter enables plastic ductility. As dislocation-enabled slip favors certain crystal orientations, dynamic recrystallization plays a role by supplying new crystal grains favorably oriented to plastic slip. It is not surprising that, as the thin sections in Figure 1 reveal, greater recrystallization was found in the more highly pre-strained specimens.

However, the factor that seems more fundamental to the observed effects of pre-strain is the accumulation of non-propagating cracks, which act to relieve local internal stresses and which create new free surfaces that serve as sources for recrystallization. Fresh-water ice that was pre-strained, for instance, by 3.5 % at $10^{-5}\,\mathrm{s}^{-1}$ appeared to contain relatively few recrystalized grains but numerous cracks (Figure 1)—its elastic moduli were reduced (Figure 2) and $\dot{\varepsilon}_{DB}$ was increased (Figure 5) by significant amounts. On the other hand, similarly pre-strained salt-water ice appeared to have relatively fewer cracks despite more recrystallization than seen in the fresh-water ice, yet the changes to elastic moduli and $\dot{\varepsilon}_{DB}$ in the saline ice were more subtle. When saline ice was pre-strained instead at $10^{-4}\,\mathrm{s}^{-1}$, more cracks developed and the magnitude of changes to moduli and $\dot{\varepsilon}_{DB}$ increased. The effects of damage then became comparable in both materials when each was pre-strained at a rate one order of magnitude below its inherent undamaged transition strain rate.

Moreover, as was mentioned with the elastic properties, there appears to be some difference in mechanical response depending on the orientation in which the specimen is reloaded. For example, consider fresh-water ice with 3.5 % pre-strain. When reloaded in x_1, i.e., parallel to the initial loading, at $3 \times 10^{-4}\,\mathrm{s}^{-1}$ (Figure 4c), a peak stress occurs near 0.5 % strain, preceded by strain hardening and followed by softening, phenomenologically identical to the behavior of un-damaged ice when loaded within the ductile regime. But for reloading in the perpendicular direction x_2, no peak stress is reached up to 3.5 % strain, the upper limit for those tests. Instead, the slope of the stress-strain curve lessens fairly abruptly around 0.25 % strain but remains posi-

tive, suggestive of an extended hardening process. The nature of this damage-induced anisotropy warrants further study. Meanwhile, these observations support the argument that recrystallized grains (which appeared equiaxed) play a lesser role than do cracks (which tended to align parallel to the pre-strain loading direction) in affecting the elastic properties and macroscopic behavior of pre-strained material.

4 CONCLUSION

The experiments reported here have established that pre-strain affects both the elastic and the inelastic behavior of columnar-grained ice that possesses the S2 crystallographic growth texture. Measurements on fresh-water material have revealed that shortening of 3.5 % to 10 % (at $-10\,^{\circ}\mathrm{C}$ at $10^{-5}\,\mathrm{s}^{-1}$ by loading uniaxially along an across-column direction) introduces a level of damage in the form of cracks and recrystallized grains that has several effects: elastic moduli are reduced by 10 % to 30 %; the strain rate that marks the ductile-to-brittle transition is increased by a factor of 3 to 10; and the ductile behavior with respect to loading along a direction within the horizontal plane of the parent ice sheet changes from isotropic to anisotropic. In saline ice (also at $-10\,^{\circ}\mathrm{C}$), the same levels of pre-strain, when imparted at $10^{-5}\,\mathrm{s}^{-1}$, reduce the elastic moduli by only 3 % to 15 %, and increase $\dot{\varepsilon}_{\mathrm{DB}}$ to a lesser degree than in fresh-water ice. However, when saline ice is pre-strained at $10^{-4}\,\mathrm{s}^{-1}$, a rate one order of magnitude below its inherent ductile-to-brittle transition, the effects of pre-strain become more pronounced and comparable to those seen in fresh-water ice pre-strained at $10^{-5}\,\mathrm{s}^{-1}$. The picture that is beginning to emerge suggests that the effects of plastic deformation damage are enhanced as the strain rate at which pre-strain is imparted approaches the ductile-to-brittle transition strain rate of the undamaged material. Future tests will explore this hypothesis.

5 ACKNOWLEDGEMENTS

We are grateful to Narayana Golding and Andrew L. Fortt for their assistance with the experimental methodology and MATS apparatus. This work was supported by the U.S. Department of the Interior–Bureau of Safety and Environmental Enforcement (BSEE), contract no. E12PC00033.

REFERENCES

Gammon, P. H., Kiefte, H. and Clouter, M. J. (1983), 'Elastic constants of ice samples by brillouin spectroscopy', *The Journal of Physical Chemistry* **87**(21), 4025–4029.

Kuehn, G., Schulson, E. and Nixon, W. (1988), The effects of prestrain on the compressive ductile-to-brittle transition in ice, *in* H. Saeki and K. i. Hirayama, eds, 'IAHR International Symposium on Ice, Proceedings Vol. I', pp. 109–17.

Lemaitre, J. (1996), *A Course on Damage Mechanics*, Springer, Berlin.

Qi, S. and Schulson, E. (1998), The effect of temperature on the ductile-to-brittle transition in columnar ice, *in* '14th International Symposium on Ice. Potsdam, NY: AA Balkema Publishers', pp. 521–7.

Schulson, E. and Buck, S. (1995), 'The ductile-to-brittle transition and ductile failure envelopes of orthotropic ice under biaxial compression', *Acta metallurgica et materialia* **43**(10), 3661–3668.

Schulson, E. M. and Duval, P. (2009), *Creep and Fracture of Ice*, Cambridge University Press.

Sinha, N. K. (1989), 'Elasticity of natural types of polycrystalline ice', *Cold Regions Science and Technology* **17**(2), 127 – 135.

Sodhi, D. S. (2001), 'Crushing failure during ice-structure interaction', *Engineering Fracture Mechanics* **68**(17), 1889–1921.

Vaudrey, K. (1977), Ice engineering - study of related properties of floating sea-ice sheets and summary of elastic and viscoelastic analyses, Technical Report R 860, Civil Engineering Laboratory, Naval Construction Battalion Center.

Weiss, J. (2001), 'Fracture and fragmentation of ice: a fractal analysis of scale invariance', *Engineering Fracture Mechanics* **68**(17-18), 1975–2012.